Cytokine therapy-mediated neuroprotection in a Friedreich's ataxia mouse model

Kevin C Kemp (MSc, PhD) [1], Nadia Cerminara (BSc, PhD) [2], Kelly Hares (BSc, PhD) [1], Juliana Redondo (BSc, PhD) [1], Amelia J Cook [1], Harry R Haynes (BSc, MBChB), [3], Bronwen R Burton (BSc, PhD) [4], Mark Pook (BSc, PhD) [5], Richard Apps (PhD) [2], Neil J Scolding (FRCP, PhD)[1] and Alastair Wilkins (FRCP, PhD)[1]*

[1.] *Multiple Sclerosis and Stem Cell Group, School of Clinical Sciences, University of Bristol.*

[2.] *Sensory and Motor Systems Group, School of Physiology, Pharmacology and Neuroscience, University of Bristol.*

[3.] *Brain Tumour research group, School of Clinical Sciences, University of Bristol.*

[4.] *Infection and Immunity, School of Cellular and Molecular Medicine, University of Bristol.*

[5.] *Synthetic Biology Theme, Institute of Environment Health & Societies, Biosciences, Dept. of Life Sciences, College of Health & Life Sciences, Brunel University London.*

Running head: Effective cytokine therapy for Friedreich's ataxia

Number of characters: Title (78), Running head (50). **Word counts:** Abstract (242), Introduction (324), Discussion (759), Body of manuscript (4792). **Number of figures:** (7), Colour (7) **Number of tables:** (1)

Contact information

Dr Kevin Kemp, Multiple Sclerosis and Stem Cell Group, University of Bristol, Clinical Neurosciences office, 1st floor, Learning and Research building, Southmead Hospital, Bristol, BS10 5NB, UK. e-mail: kevin.kemp@bristol.ac.uk tel: +44 117 4147817

This article has been accepted for publication and undergone full peer review but has not been through the copyediting, typesetting, pagination and proofreading process which may lead to differences between this version and the Version of Record. Please cite this article as an 'Accepted Article', doi: 10.1002/ana.24846

Abstract

Objectives: Friedreich's ataxia is a devastating neurological disease currently lacking any proven treatment. We studied the neuro-protective effects of the cytokines granulocyte-colony stimulating factor and stem cell factor in a humanised murine model of Friedreich's ataxia.

Methods: Mice received monthly subcutaneous infusions of cytokines while also being assessed at monthly time points using an extensive range of behavioural motor performance tests. After 6 months of treatment, neurophysiological evaluation of both sensory and motor nerve conduction was performed. Subsequently, mice were sacrificed for mRNA, protein and histological analysis of the dorsal root ganglion, spinal cord and cerebellum.

Results: Cytokine administration resulted in significant reversal of biochemical, neuropathological, neurophysiological and behavioural deficits associated with Friedreich's ataxia. Both granulocyte-colony stimulating factor and stem cell factor had pronounced effects on frataxin levels (the primary molecular defect in the pathogenesis of the disease), and on regulators of frataxin expression. Sustained improvements in motor coordination and locomotor activity were seen, even after onset of neurological symptoms. Treatment also restored the duration of sensory nerve compound potentials. Improvements in peripheral nerve conduction positively correlated with cytokine-induced increases in frataxin expression, providing a link between increases in frataxin and neurophysiological function. Abrogation of disease-related pathology was also evident, with reductions in inflammation/gliosis and increased neural stem cell numbers in areas of tissue injury.

Interpretation: These experiments show that cytokines already clinically used in other conditions offer the prospect of a novel, rapidly translatable, disease-modifying and neuroprotective treatment for Friedreich's ataxia.

Introduction

Friedreich's ataxia, the commonest autosomal recessive ataxic condition, is characterised neuropathologically by degeneration of large sensory neurons, the spinal cord and the deep cerebellar nuclei [1]. Friedreich's ataxia patients inevitably acquire neurological disability, with progressive ataxia, dysarthria, neuropathy and pyramidal weakness, as well as cardiac and endocrine disease [2]. In most cases, Friedreich's ataxia is caused by homozygous GAA.TCC tri-nucleotide repeat expansion within intron 1 of the *FXN* gene [3] causing transcriptional repression of frataxin [4]. Frataxin is an essential mitochondrial protein, loss of which causes disrupted respiratory chain activity, impaired cellular iron homeostasis and oxidative stress, leading to cell death in affected tissues [5-7].

Currently, there are no treatments that can protect nerves, promote nervous system regeneration, or slow disease progression [8]. However, specific cytokines and growth factors may show therapeutic potential in mediating nervous system injury and repair. Originally used clinically for stimulating and mobilising specific sub-sets of bone marrow stem and progenitor cell populations prior to a peripheral blood stem cell harvest, the agents granulocyte-colony stimulating factor (G-CSF) and stem cell factor (SCF) [9, 10], may also exhibit direct protective and reparative effects within diseased tissues; and in combination, show significant biological and clinical synergy with one another [11]. Therapeutically, G-CSF and SCF are known to cross the blood brain barrier [12], exert anti-apoptotic effects on glial and/or neural cells [13, 14], stimulate neurogenesis and neurite outgrowth [15, 16], and promote migration of endogenous neural progenitor cells [17]. Furthermore, these agents promote accelerated recovery in several animal models of neurological disease [18] and are already in human clinical trials for other neurological disorders [19]. Here, we study the therapeutic potential of the repeated subcutaneous administration of both G-CSF and SCF in a humanised

murine Friedreich's ataxia model. Using recognised cytokine regimens for the mobilisation of murine peripheral blood hematopoietic stem cells (HSCs) we demonstrate for the first time major benefits in clinical, biochemical, neurophysiological and pathological parameters associated with the disease.

Methods

Experimental design

The objectives of the study were to investigate, in a mouse model of Friedreich's ataxia (YG8R mice), the therapeutic effects of cytokine administration (G-CSF/SCF) on disease phenotype. Experimental protocols are described in **Fig 1A.** Investigators were blinded to treatment group for behavioural studies.

Animals

All animal experiments were performed in accordance with the UK Animals (Scientific Procedures) Act 1986 and approved by the University of Bristol Animal Welfare and Ethical Review Body. *Fxn*^{tm1Mkn} Tg(FXN)YG8Pook/J (YG8R) transgenic mice, which carry a human genomic *FXN* transgene (on a murine frataxin null background) containing expanded GAA repeats of 82-190 units within intron 1 of *FXN* were used. Ataxic (strain# *Fxn*^{tm1Mkn} Tg(FXN)YG8Pook/J, stock # 008398) were purchased from Jackson Laboratory, US. Control C57BL/6 VAF/Elite mice were provided by Charles River, UK. All mice were housed in a pathogen-free facility, with free access to food and water.

Treatment

Cytokines doses were based on standard regimens for G-CSF mobilisation of peripheral blood HSCs. In humans, 5-10 µg kg day of recombinant G-CSF is administered for 4-7 days (British National Formulary; BNF [20]). Mobilising doses of G-CSF for murine HSC is considerably higher than for humans to achieve similar levels of mobilisation [21], commonly 100-300 µg kg day is injected for five or more days [22-24]. The rationale to use cytokines G-CSF and SCF at a single fixed dosage (200 µg per kg) was to allow comparisons to be made between the effectiveness of the two cytokines when used alone.

Mice received subcutaneous injection of murine G-CSF and/or SCF (Peprotech; both 200 µg per kg) in phosphate-buffered saline (PBS) once daily for five consecutive days. Treatments were repeated every four weeks. PBS alone was administered as a vehicle control, during the same period. Bromodeoxyuridine (BrdU) (Sigma-Aldrich; 50 mg per kg) in PBS was also administered intraperitoneally once daily for five consecutive days (directly following growth factor infusion) during the last treatment round.

Peripheral blood mononuclear cell counts

One hundred microliters of peripheral blood was harvested from the tail vein and suspended in PBS pH 7.4/EDTA (2 mg/ml). Red cells were removed using red cell lysis buffer, the remaining nucleated cell population re-suspended in PBS/3% foetal bovine serum (FBS) and counted using a haemocytometer.

Neurobehavioral testing

Body Weight

Mouse body weights were recorded once monthly between 3-9 months of age using a digital scale.

Rotarod

A digital rotarod, rod diameter 30 mm, accelerating from 4 to 40 rpm over 400 s was used. (Ugo Basile 47600) Mice were allowed to stand on the slowly rotating (4 rpm) rod for 30s before acceleration. Each month, mice were first trained on the rotarod using three unrecorded trials with 15min inter-trial intervals. Six hours later, mice received four recorded trials with 15min inter-trial intervals. All trials ended when the mouse fell off the rotarod or after a maximum 400s had elapsed. The time that each mouse maintained its balance on the rotating rod was measured as the latency to fall.

Grip Strength

A 2.5 Newton meter was used to assess the forelimb grip strength. Mice were held by the base of the tail and allowed to grasp a metal bar attached to the meter. The peak force with which mice pulled the bar horizontally was measured in three trials with a rest period of 1 minute between each trial.

Bar hang test

Mice were placed with their forepaws grasping the middle of a 200mm horizontal wooden bar (4mm thick), secured to a vertical post, elevated 300mm from a flat surface. The ability to grip the bar was scored as following: 0 unable to remain on bar; 1 hangs by both forepaws; 2 attempts to climb onto bar; 3 both forepaws and one or both hind paws around bar; 4 four paws and tail around bar, with lateral movement; 5 escape. The score was measured in three trials with a rest period of 5 minutes between each trial.

String test

Mice were placed with their forepaws grasping the middle of a taut 1m horizontal rope (4mm thick), suspended between two vertical supports, elevated 300mm from a flat surface. The time taken for each mouse to reach either end of the rope was measured. Trials ended when the mouse fell off the rope or after a maximum 60s had elapsed. Latency was measured in three trials with a rest period of 5 minutes between each trial.

Beam-walk test

The test was carried out using a wooden beam 900mm long, with an external diameter of 10mm. Within a darkened room, the beam was placed between two platforms sloping up from 300mm to 600mm above the bench surface with lower end mounted on a narrow support with a 60W lamp, while a darkened safety platform was located at the other end of the beam, in which the mouse could escape. Performance on the beam was quantified by measuring the time it took the mouse to traverse the beam and enter the safety platform. The latency was measured with a rest period of 5 minutes between each trial.

Open field

Within a darkened room, mice were placed into a 3 x 3 gridded (300 x 300mm size) clear Perspex box with 150mm high walls. A 60W lamp illuminated the arena. The total number of grid squares entered, the frequency of central square entered and the total number of hind-paw rearings by each mouse over a period of 5 minutes was recorded. Scores were measured with a rest period of 30 minutes between each trial

Gait analysis

To obtain footprints, the hind- and forepaws of the mice were coated with red and green nontoxic food colouring, respectively. The animals were then allowed to walk along a

500mm long, 55mm wide runway with 100mm high walls (lit at the entrance with a 60W lamp), with white paper lining the floor, into a darkened enclosed escape box. All mice received both one training and trial run. A fresh sheet of paper was placed on the floor of the runway for each run. The footprint patterns of the hind- and forepaws were analysed for four step parameters (all measured in millimetres): stride length, stance length, intra-step length and overlap distance (shown in **Fig 2**).

Neurophysiology

Animals were anaesthetised with ketamine (100mg/kg, Vetalar, Boehringer Ingelheim Vetmedica Inc., Missouri USA) and xylazine (10mg/kg, Rompun, Bayer, Berkshirem UK) intraperitoneally. The depth of anaesthesia was regularly assessed by a paw pinch to monitor reflex muscle tone and supplementary doses were administered as required. Core body temperature was maintained at 37°C by a heated blanket.

Tail nerve conduction studies

Assessment of the conduction velocity of sensory and motor fibres was performed by stimulating the distal and proximal parts of the tail respectively, and recording evoked responses [25, 26]. For stimulation of the sensory nerves, two uninsulated needles with a separation of approximately 5mm were inserted at the tip of the tail with the cathode. The cathode was the most proximal of the needles to the base of the tail. Bipolar recordings were made using needle electrodes inserted approximately 20 mm (Position A) and 40 mm (Position B) from the cathode. The reference electrode was inserted above the base of the tail. For stimulation of motor nerves, the same electrode positions were used except that the

electrodes in the tip of the tail were used to record the responses and stimulation delivered at Positions A and B.

Electrical stimulation consisted of constant current square pulses of 0.2ms duration delivered every 3s. Recordings were made with a stimulus intensity x3 threshold to evoke a response. The nerve compound potentials were amplified (x1000), bandpass filtered (5Hz to 5kHz) and digitized on-line using a Cambridge Electronic Design (CED, Cambridge, UK) Micro 1401 analog-to-digital converter and Spike2 software (CED). The latency of the responses was taken from stimulus onset time to the beginning of the potential as well as to the peak. The distance between the two recording sites was measured with a calliper and the sensory and motor nerve conductions calculated by dividing the distance by the difference in latencies of the proximal and distal recording sites. For each animal analysis of sensory and motor conduction velocities and nerve volley duration was based on an average of 10 trials.

Tissue processing

Mice were sacrificed and tissues for both proteomic and genomic analyses were dissected, immediately snap-frozen in liquid nitrogen and stored at -80ºC until use. Frozen tissue was then thawed and homogenized on ice by use of the PARIS kit (Ambion, UK) and a protease and phosphatase inhibitor cocktail (1:100; Thermo Scientific, UK).

For histological analyses, mice were anaesthetised by intraperitoneal injection of Euthatal and perfused with PBS followed by 4% paraformaldehyde in PBS. The brains and spinal cords were dissected and placed in 4% paraformaldehyde in PBS for 24h at 4°C and subsequently embedded in paraffin for sectioning on a rotary microtome (Leica LM2135) and mounting on glass slides.

Gene expression analysis: Quantitative PCR

Total RNA was extracted from tissue lysates on ice using the PARIS kit (Ambion, UK) according to manufacturer's instructions and treated with DNase I recombinant (Roche)/$MgCl_2$ solution (Quantace). All RNA samples were quantified using a Qubit Fluorometer and Quant-iT RNA assay kit (Invitrogen, Paisley, UK) according to manufacturers' instructions. RNA was reverse transcribed to produce cDNA using the High Capacity cDNA Kit (Applied Biosystems, Foster City, CA, USA) and qPCR performed using TaqMan Fast Advanced Master Mix (Applied Biosciences) and StepOnePlus™ Real-Time PCR System (Applied Biosystems, UK) with primers for *Epas1* (Mm01236112_m1), *FXN* (Hs00175940_m1), *Srf* (Mm00491032_m1), *Tfap2a* (Mm00495574_m1); *Trp53* (Mm01731290_g1) (TaqMan MGB probe, FAM dye-labelled, Applied Biosystems, Paisley, UK). The relative gene expression (RQ value) was calculated using the $2^{-\Delta\Delta Ct}$ method with both Beta Actin (*Actb;* Mm00607939_s1) and NeuN (Rbfox3; Mm01248771_m1) used as housekeeping genes.

Protein analysis

The Qubit ® Fluorometer and Quant-iT™ protein assay kit (Invitrogen, UK) was used to quantify the concentration of total protein within each tissue homogenate. Frataxin levels were measured using the Frataxin Human SimpleStep ELISA kit (Abcam) and the enzyme activity of Aconitase was determined using the Aconitase assay kit (Caymen Chemical).

For further quantitative protein analysis, immuno dot-blotting was carried out using the Bio-Dot Microfiltration manifold system (Biorad). Protein homogenates were transferred to the nitrocellulose membrane using gravity filtration, blocked using 5% BSA, before incubation with the following primary antibodies:- Catalase (Abcam; ab16731 1:5000), GPX1 (Abcam; ab22604 1:5000), 4-HNE (Abcam; ab48506 1:6000), Nrf2 (Santa Cruz; sc-722 1:2000), PGC-1a (Santa Cruz; sc-13067 1:2000), NeuN (Abcam; ab177487 1:4000), SOD1 (Abcam;

ab16831 1:5000), SOD2 (Abcam; ab16956 1:20000). Immunoreactivity was detected using HRP-conjugated goat anti-mouse IgG (1:5000; Ab6789) or anti-rabbit IgG (1:3000; Ab6721) secondary antibodies (Abcam). Protein expression was visualised using a chemiluminescence EZ-ECL kit in conjunction with a Biorad Universal III Bioplex imager. Densitometric analysis of protein expression was performed using Image Lab™ 5.0 software (Biorad).

Immunohistochemistry and imaging

Mounted tissue sections were deparaffinised, hydrated and washed with PBS. For antigen-exposing pre-treatment, sections were incubated with boiling 0.01M Sodium Citrate buffer pH 6.0. Immunohistochemical staining with DAB has been described previously [27]. For immunofluorescent labelling, non-specific binding was blocked with 10% normal goat serum diluted in PBS containing 0.1% triton. Sections were incubated at 4°C overnight with primary antibodies to 4-HNE (Abcam; ab48506 1:200), Beta-3 tubulin (Abcam; ab78078 1:250), BrdU (Sigma-Aldrich; B2531), Calbindin-D28K (Sigma-Aldrich; C2724 1:500), GAD (Abcam; ab11070 1:1000), GFAP (Abcam; ab33922 1:200), MBP (Serotec; MCA4095 1:100), NeuN (abcam; ab177487 1:500 & ab104224 1:500), Nestin (BD bioscience; 556309 1:200), OX42 (Abcam; ab1211 1:100), S100 (Milipore; MAB079 1:200), S100 (Dako; Z0311 1:200). Sections were washed in PBS and incubated for 45 minutes in the dark with Alexa Fluor 488/555, goat anti-mouse (1:500) or Alexa Fluor 488/555, goat anti-rabbit (1:500) (Invitrogen, Paisley, UK), before being mounted in Vectashield medium containing the nuclear dye 4′6′-diamidino-2-phenylindole (DAPI) (H-1200, Vector Laboratories). For BrdU labelling, sections were incubated at 37°C in 2N HCl for 30 mins followed by 0.1% Trypsin for 20 mins prior to blocking.

Confocal analysis was performed using either a Leica SP5-AOBS confocal laser scanning microscope attached to a Leica DM I6000 inverted epifluorescence microscope; or a Nikon C1 confocal microscope and EZ viewer software. All Z-stack and 3-dimensional imaging was created using both Leica Application Suite Advanced Fluorescence software and Volocity 3D image software (PerkinElmer, USA). For light imaging, images were acquired using an Olympus IX70 microscope coupled with Image-Pro Plus software.

Histological staining

For histological assessment, tissues were sectioned, deparaffinated, hydrated, and stained with hematoxylin and eosin (H&E) (visualisation of dorsal root ganglion (DRG) vacuoles) or Luxol fast blue/cresyl violet (visualisation of myelin).

Cell quantification

At least four independent tissue samples from each group were included in the analyses. All cells were counted within randomly assigned set areas within the DRG, spinal cord and dentate nucleus. For spinal cord sections, representative samples of cervical, thoracic and lumbar were all analysed.

DRG Vacuoles

Each section was scanned across the entire cross-sectional area of the DRG for neuronal cell bodies containing either nuclear and/or cytoplasmic vacuoles. A minimum of 400 DRG neurons from each mouse was examined, allowing for the determination of the frequency of vacuolated cells.

Neuronal cell size

To quantify changes in neuronal size, the cross-sectional diameter of a nucleated cell soma was measured in each cell using ImageJ software. Neurons were identified by either Beta-3 tubulin (dentate nucleus) or NeuN/H&E (DRG).

Statistical analysis

The analysis was performed using GraphPad Prism (GraphPad Software Inc, USA). For all tests, values of $p<0.05$ were considered statistically significant. Statistical tests were all two-sided. At least 5 independent tissue samples or mice from each group were included in the analyses. Data between two groups were analysed using either unpaired t-tests or Mann-Whitney U tests. Statistical comparisons for over two groups were analysed using either Friedman test, one-way or two-way analysis of variance (ANOVA) with *post hoc* testing between groups where appropriate (as indicated in figure legends). Where possible, data are represented as mean ± SEM, or for qPCR data geometric mean ± 95% confidence intervals are stated.

Results

To investigate G-CSF/SCF administration, we used three month *Fxn*^{tm1Mkn} Tg(FXN)YG8Pook/J (YG8R) transgenic mice, which carry human genomic *FXN* transgene (on a murine frataxin null background) containing a GAA expansion within intron 1. Mice are frataxin-deficient and develop progressive neurodegeneration and cardiac pathology [28, 29]. Due to the phenotypic similarity between C57BL/6 and Y47R (containing the human *FXN* transgene with normal-sized GAA repeats) mice, C57BL/6 mice were used as healthy

controls [29]. Before any therapeutic intervention, neurological deficits were already apparent in the YG8R mice compared to age-matched wild-type controls. These deficits in the YG8R mice became more prominent with increasing age (**Fig 1C to H, Fig 2**).

(a) G-CSF and SCF improve both motor and locomotor performance in YG8R mice

YG8R transgenic mice were subcutaneously injected with PBS (controls) or G-CSF and/or SCF dissolved in PBS (daily for five consecutive days) monthly for six consecutive months (**Fig 1A**). For the duration of the study, no observable side effects in the mice were noted post G-CSF and/or SCF administration, weights remained consistent/normal (**Fig 3B**) and all mice (n = 50) completed the study. Combined G-CSF/SCF increased peripheral blood MNC counts approximately 8-fold, and was a more effective mobilising regimen compared to administration of single agents (**Fig 3A**).

Motor coordination and locomotor activity in YG8R and Control mice was assessed monthly. Significantly, after six months of G-CSF and/or SCF administration, improvements were seen in the majority of motor coordination and locomotor activities tested **(Fig 3C to I**). Performances were independent of changes in body mass (**Fig 3B**).

(b) G-CSF and SCF increase frataxin mRNA and protein expression

Transcriptional repression of *FXN* is the primary molecular event in the pathogenesis of Friedreich's ataxia [3, 4]. To explore potential neuroprotective mechanisms of G-CSF and SCF, we measured frataxin mRNA levels in cerebellum and spinal cord of YG8R mice (aged 9 months) 24 hours post-injection of cytokines. *FXN* mRNA levels were significantly amplified following treatment, with G-CSF or G-CSF/SCF (cerebellum) and G-CSF/SCF (spinal cord)

having the most pronounced effects (**Fig 4B**). Notably, in all cases increases in frataxin mRNA expression were more prominent using the neuronal specific marker NeuN housekeeping gene comparator, suggesting that the treatments, at least in part, potentiate increases in neuronal frataxin.

Transcriptional repression of *FXN* is thought to result from reduced accessibility of transcriptional regulatory factors to the promoter region caused by the tri-nucleotide repeat expansion [30], and various regulatory factors binding close to the *FXN* gene locus are implicated [31-33] (**Fig 4A**). Of these, we found that Tumour Protein p53 (p53; encoded by *Trp53)*, Transcription Factor AP-2 alpha (TFAP2A; encoded by *Tfap2a*), Serum Response Factor (SRF; encoded by *Srf*) and Hypoxia-Inducible Factor-2alpha (HIF-2A; encoded by *Epas1*) were increased following cytokine administration (**Fig 4C**). Of the regulatory factors tested, only *Epas1* and *Trp53* were upregulated in both cerebellum and spinal cord in response to cytokine administration; and of these only *Epas1* expression in treated mice correlated with respective *FXN* expression **Fig 4D**.

We also showed marked increases in frataxin protein expression within the spinal cord, and to a lesser extent in the cerebellum, with G-CSF or G-CSF/SCF administration (using a human-specific frataxin ELISA, as with qPCR analysis, did not allow comparisons between the 'human' frataxin levels within YG8R mice and control mouse frataxin levels; **Fig 4B**).

Frataxin deficiency results in increased oxidative stress and impaired recruitment of antioxidant defences [34]. YG8R mice have reduced protein levels of Peroxisome proliferator-Activated Receptor gamma coactivator 1-alpha (PGC-1a) and Nuclear Factor (erythroid-derived 2)-like 2 (Nrf2) in either the spinal cord and/or cerebellum [35, 36]. This was associated

with global reductions in expression of anti-oxidant enzymes and enzymatic activity of the iron-sulphur protein aconitase within the cerebellum [28] (**Table 1**). Untreated YG8R mice showed increases in the lipid peroxidation product 4-HNE, within cerebellum and spinal cord (**Table 1**).

Administration of cytokines led to restoration of aconitase activity in cerebellum and spinal cord to, or beyond, levels seen in wild-type control mice. Similarly, there were increases in levels of PGC-1a and Nrf2 protein expression with associated elevations in superoxide dismutase 1 and 2 (SOD1 and SOD2), catalase and glutathione peroxidase. Finally, consistent with cytokines facilitating redox homeostasis, in cerebellum and spinal cord, reductions in 4-HNE were also apparent with combined administration of G-CSF and SCF (**Table 1**).

(c) G-CSF and SCF improve nerve conduction

Since Friedreich's ataxia patients exhibit abnormalities in nerve conduction [37], neurophysiological evaluation of sensory and motor nerve conduction was performed. Electrophysiological recordings were obtained from the tail nerves of wild-type controls, untreated YG8R mice and YG8R mice treated with combined G-CSF/SCF (**Fig 5A to D**). There was no statistical difference in the sensory or motor conduction velocities among all three groups regardless of whether the peak (**Fig 5C**) or onset latency was used. However, the duration of the sensory compound nerve potential in untreated YG8R mice was significantly longer than that of wild-type controls, signifying temporal dispersion of the nerve impulses evoked by the stimulation. Furthermore, G-CSF/SCF treatment restored nerve volley duration to normal levels (**Fig 5C**).

Electrophysiological abnormalities in Friedreich's ataxia correlate with GAA triplet repeat expansion length [38] (and therefore reduced frataxin protein expression). We found that

increases in cerebellar frataxin protein levels in G-CSF/SCF treated mice significantly correlated with shorter duration and increased conduction velocity of sensory compound nerve potentials (**Fig 5D**). These findings provide support for a link between increases in frataxin and neurophysiological improvements observed in treated YG8R mice.

(d) G-CSF and SCF reduce DRG, spinal cord and cerebellar Friedreich's ataxia-related pathology

We further characterised neuropathological changes in YG8R mice. In common with human Friedreich's ataxia [1] and previous studies describing the YG8R mouse [28, 39], untreated YG8R mice displayed: frequent intra-nuclear and intra-cytoplasmic vacuolisation of the large sensory neuronal cell bodies of the dorsal root ganglia (DRG) with significant lipofuscin accumulation (**Fig 6A to D**) and an increased satellite cell to DRG neuron ratio (**Fig 6E**) representing large sensory DRG neuronal loss (**Fig 6F to G**) and/or subsequent satellite cell proliferation; neuronal loss in the spinal cord dorsal nucleus of Clarke (DNoC) (**Fig 6H to I**); atrophy of large neurons within the cerebellar dentate nucleus with grumose-type glutamic acid decarboxylase (GAD) positive intracytoplasmic labelling pattern in the large neuronal cell bodies of the YG8R (**Fig 6J to M**); spinal cord astrocytosis associated 4-Hydroxynonenal (4-HNE) accumulation at the peripheral aspects of the anterior and lateral white matter tracts and extending into the dorsal columns **(Fig 7C, D, G)**, although no significant white matter loss (**Fig 7E to F**). Patchy astrocytosis was also seen in the grey matter surrounding the central canal and extending towards the DNoC (**Fig 7G**); influx of inflammatory OX42 (CD11b/c) positive cells in both the spinal cord and dentate nucleus (**Fig 7A to B**); and reduction in nestin-positive cells in lateral corticospinal tracts, DNoC and dentate nucleus, compared to wild-type control mice (**Fig 7H to I**).

We observed clear attenuation of Friedreich's ataxia-associated pathology within the DRG, spinal cord and cerebellum of YG8R mice treated with cytokines. All treatment regimens led to significant reductions in the number of DRG neurons containing either intra-cytoplasmic or intra-nuclear vacuoles (**Fig 6A to C**). Furthermore, treatment returned satellite-cell-to-neuronal ratios to levels found in wild-type controls - a likely consequence of improved large sensory neuronal cell survival (**Fig 6E to G**). Combined G-CSF/SCF treatment markedly reduced neuronal loss within the spinal cord DNoC (**Fig 6H to I**); and reduced the extent of astrocytosis and inflammatory cell infiltrate within dorsal columns, spinocerebellar and corticospinal tracts (**Fig 7A to D**). In the dentate nucleus, both G-CSF and SCF reduced atrophy of large neurons (resulting in an increased mean neuronal cell size) and reduced the presence of grumose degeneration (**Fig 6J to M**).

To assess the effects of treatment on cellular kinetics, YG8R mice were injected with the thymidine analogue 5-bromo-2'-deoxyuridine (BrdU) directly following cytokine treatment during the final treatment round (**Fig 1A**). Histological analysis one month post-BrdU revealed a distinct reduction in BrdU cell numbers within DRG of untreated YG8R mice (compared to wild-type controls) but marked increases in BrdU cells in DRG, dorsal spinal roots, dentate nucleus, and to a lesser extent in the spinal cord in G-CSF and/or SCF-treated mice (**Fig 7J**). We also found the pool of nestin-positive neural precursor cells within the DRG, spinal cord and dentate nucleus was significantly amplified in response to treatment with G-CSF and/or SCF (**Fig 7H to I**).

Discussion

Here we show that administration of G-CSF and SCF have marked direct neuroprotective effects in a 'humanised' mouse model of Friedreich's ataxia; these agents correct many Friedreich's ataxia-associated biochemical abnormalities and improve functional, neurophysiological and pathological parameters. Significantly, administration of G-CSF and/or SCF mediates sustained improvements in motor coordination and locomotor activity in YG8R 'Friedreich's' mice, even after onset of clinical symptoms. Treatment also restored the duration of sensory nerve compound potentials, reflecting reduced variability in conduction velocities of individual nerve fibres associated with Friedreich's ataxia dysfunction [37, 38].

G-CSF and SCF had pronounced effects on frataxin levels, and on regulators of frataxin expression within both the cerebellum and spinal cord. Of the potential transcription factors we tested [31-33], HIF-2alpha encoded by *Epas1* was upregulated in the cerebellum and spinal cord in response to treatment and correlated with *FXN* expression, highlighting a possible regulatory mechanism by which G-CSF and SCF control frataxin expression. Indeed, others have shown that HIF-2alpha can activate the murine *FXN* promoter through binding to a consensus HIF-responsive enhancer element (HRE), and mice lacking *Epas1* have markedly reduced levels of frataxin [33].

Interventions that increase the amount of the frataxin protein are attractive therapeutic approaches. Carriers of the GAA expansion, having approximately 50% of normal frataxin expression, are asymptomatic [5, 40]. Increasing cellular frataxin levels above a specific threshold therefore hold promise; a recent proof-of-concept study introducing *FXN* transgenes into heart cells of frataxin-deficient mice led to overexpression of frataxin and sustained remission of Friedreich's ataxia-associated heart disease [41]. Experimentally several

agents have shown potential to increase frataxin expression (recombinant erythropoietin, interferon-gamma, nicotinamide and resveratrol), however there has been limited success in their capacity to elevate frataxin levels when tested clinically [42-45].

Molecules coupled with frataxin deficiency were also elevated in response to treatment. Specifically, G-CSF and/or SCF increased expression of molecules associated with frataxin antioxidant functions including Nrf2, superoxide dismutases, catalase and glutathione peroxidase. Nrf2 is a key orchestrator of cellular anti-oxidant responses and its expression/activity is reduced in frataxin-deficient cells leading to increased oxidative injury [35, 46, 47]. Cytokines also increased expression of PGC-1a, another key regulator of cellular redox homeostasis [48], and reduced lipid peroxidation products [49], thus confirming their anti-oxidative effects.

YG8R mice replicate human disease in many histological aspects, with neuronal atrophy in the DRG, DNoC and dentate nucleus. Importantly, repeated administration of cytokines led to significant amelioration in disease-related pathology throughout the nervous system, the likely explanation for the observed improvements in motor and locomotor function. Mechanistically, in addition to restoring frataxin-associated cellular homeostasis, G-CSF/SCF attenuating inflammation (both astro- and microgliosis) in the nervous system of YG8R mice may have also slowed the progression of the disease [50].

Adult neurogenesis appears to be an important mechanism of brain plasticity in brain repair after injury [51]. We found reduced numbers of proliferating cells and neural precursors throughout the nervous system of untreated YG8R mice. This may be a consequence of

mitochondrial dysfunction induced by frataxin deficiency [52] and abnormal neurogenesis may, in turn, exacerbate neuropathology [53]. Both G-CSF and SCF regulate proliferation, differentiation and recruitment of endogenous neural and BM progenitor cells during neurological injury [17, 54]. In accordance, cytokine administration increased the number of both nestin-positive and proliferating cells in the YG8R nervous system. Of note, numbers of nestin cells were elevated in the DRG, DNoC and dentate nucleus, all areas in which neuronal preservation was apparent in response to treatment.

As demonstrated here, humanised mice are powerful tools in pre-clinical testing of potential therapeutic agents of neurological disease; however, care should be taken when interpreting data due to underlying genomic differences between rodents and humans. We believe these observations warrant further clinical trials of stem cell mobilising agents in patients with Friedreich's ataxia. When used clinically, both G-CSF and SCF are generally well tolerated with G-CSF having a well-established safety record in healthy peripheral blood stem cell donors. The pharmacokinetics of G-CSF administration has been extensively studied in humans and the therapeutic window, in terms of achieving HSC mobilisation, can extend beyond twice the recommend dose [55]. Furthermore, monthly administrations of mobilising agents have been shown to be safe in a trial for amyotrophic lateral sclerosis [19]. This has provided early safety data on the use of G-CSF for neurodegenerative conditions.

In conclusion, these experiments have elucidated mechanisms of action of cytokines in a 'humanised' Friedreich's ataxia mouse model. Their pleiotropic effects contribute to neuroprotection and repair against Friedreich's ataxia-associated pathological mechanisms,

thereby offering a therapy that may reduce or even help reverse long-term disability in patients with Friedreich's ataxia.

Acknowledgments

This work was supported by the Medical Research Council (grant number: MR/J012580/1)

Authors contributions

K.K, N.C, R.A, M.P, N.S and A.W:- Conception and design of the study.

K.K, N.C, R.A, K.H, J.R, A.C, H.H and B.B:- Acquisition and analysis of data.

K.K, A.W, N.S, N.C and R.A:- Drafting a significant proportion of the manuscript.

Conflicts of Interest

Nothing to report.

References

1. Koeppen AH. Friedreich's ataxia: pathology, pathogenesis, and molecular genetics. J Neurol Sci. 2011 Apr 15;303(1-2):1-12.

2. Harding AE. Friedreich's ataxia: a clinical and genetic study of 90 families with an analysis of early diagnostic criteria and intrafamilial clustering of clinical features. Brain : a journal of neurology. 1981 Sep;104(3):589-620.

3. Campuzano V, Montermini L, Molto MD, et al. Friedreich's ataxia: autosomal recessive disease caused by an intronic GAA triplet repeat expansion. Science. 1996 Mar 8;271(5254):1423-7.

4. Bidichandani SI, Ashizawa T, Patel PI. The GAA triplet-repeat expansion in Friedreich ataxia interferes with transcription and may be associated with an unusual DNA structure. Am J Hum Genet. 1998 Jan;62(1):111-21.

5. Campuzano V, Montermini L, Lutz Y, et al. Frataxin is reduced in Friedreich ataxia patients and is associated with mitochondrial membranes. Human molecular genetics. 1997 Oct;6(11):1771-80.

6. Rouault TA. Biogenesis of iron-sulfur clusters in mammalian cells: new insights and relevance to human disease. Dis Model Mech. 2012 Mar;5(2):155-64.

7. Gonzalez-Cabo P, Palau F. Mitochondrial pathophysiology in Friedreich's ataxia. Journal of neurochemistry. 2013 Aug;126 Suppl 1:53-64.

8. Corben LA, Lynch D, Pandolfo M, Schulz JB, Delatycki MB, Clinical Management Guidelines Writing G. Consensus clinical management guidelines for Friedreich ataxia. Orphanet J Rare Dis. 2014;9:184.

9. Begley CG, Basser R, Mansfield R, et al. Enhanced levels and enhanced clonogenic capacity of blood progenitor cells following administration of stem cell factor plus granulocyte colony-stimulating factor to humans. Blood. 1997 Nov 1;90(9):3378-89.

10. Shpall EJ, Wheeler CA, Turner SA, et al. A randomized phase 3 study of peripheral blood progenitor cell mobilization with stem cell factor and filgrastim in high-risk breast cancer patients. Blood. 1999 Apr 15;93(8):2491-501.

11. Duarte RF, Frank DA. SCF and G-CSF lead to the synergistic induction of proliferation and gene expression through complementary signaling pathways. Blood. 2000 Nov 15;96(10):3422-30.

12. Zhao LR, Navalitloha Y, Singhal S, et al. Hematopoietic growth factors pass through the blood-brain barrier in intact rats. Exp Neurol. 2007 Apr;204(2):569-73.

13. Schneider A, Kruger C, Steigleder T, et al. The hematopoietic factor G-CSF is a neuronal ligand that counteracts programmed cell death and drives neurogenesis. J Clin Invest. 2005 Aug;115(8):2083-98.

14. Dhandapani KM, Wade FM, Wakade C, Mahesh VB, Brann DW. Neuroprotection by stem cell factor in rat cortical neurons involves AKT and NFkappaB. Journal of neurochemistry. 2005 Oct;95(1):9-19.

15. Jin K, Mao XO, Sun Y, Xie L, Greenberg DA. Stem cell factor stimulates neurogenesis in vitro and in vivo. J Clin Invest. 2002 Aug;110(3):311-9.

16. Su Y, Cui L, Piao C, Li B, Zhao LR. The effects of hematopoietic growth factors on neurite outgrowth. PLoS One. 2013;8(10):e75562.

17. Kawada H, Takizawa S, Takanashi T, et al. Administration of hematopoietic cytokines in the subacute phase after cerebral infarction is effective for functional recovery facilitating proliferation of intrinsic neural stem/progenitor cells and transition of bone marrow-derived neuronal cells. Circulation. 2006 Feb 7;113(5):701-10.

18. Duning T, Schiffbauer H, Warnecke T, et al. G-CSF prevents the progression of structural disintegration of white matter tracts in amyotrophic lateral sclerosis: a pilot trial. PLoS One. 2011;6(3):e17770.

19. Grassinger J, Khomenko A, Hart C, et al. Safety and feasibility of long term administration of recombinant human granulocyte-colony stimulating factor in patients with amyotrophic lateral sclerosis. Cytokine. 2014 May;67(1):21-8.

20. British Medical Association, Royal Pharmaceutical Society of Great Britain. British national formulary : BNF. 70 September 2015-March 2016. London: BMA, Royal Pharmaceutical Company; 2015.

21. Zaucha JM, Knopinska-Posluszny W, Bieniaszewska M, Mysliwski A, Hellmann A. The effect of short G-CSF administration on the numbers and clonogenic efficiency of hematopoietic progenitor cells in bone marrow and peripheral blood of normal donors. Ann Transplant. 2000;5(4):20-6.

22. Roberts AW, Foote S, Alexander WS, Scott C, Robb L, Metcalf D. Genetic influences determining progenitor cell mobilization and leukocytosis induced by granulocyte colony-stimulating factor. Blood. 1997 Apr 15;89(8):2736-44.

23. Christopher MJ, Rao M, Liu F, Woloszynek JR, Link DC. Expression of the G-CSF receptor in monocytic cells is sufficient to mediate hematopoietic progenitor mobilization by G-CSF in mice. J Exp Med. 2011 Feb 14;208(2):251-60.

24. Winkler IG, Pettit AR, Raggatt LJ, et al. Hematopoietic stem cell mobilizing agents G-CSF, cyclophosphamide or AMD3100 have distinct mechanisms of action on bone marrow HSC niches and bone formation. Leukemia. 2012 Jul;26(7):1594-601.

25. Leandri M, Saturno M, Cilli M, Bisaglia M, Lunardi G. Compound action potential of sensory tail nerves in the rat. Exp Neurol. 2007 Jan;203(1):148-57.

26. Leandri M, Ghignotti M, Emionite L, Leandri S, Cilli M. Electrophysiological features of the mouse tail nerves and their changes in chemotherapy induced peripheral neuropathy (CIPN). J Neurosci Methods. 2012 Aug 15;209(2):403-9.

27. Kemp K, Gray E, Wilkins A, Scolding N. Purkinje cell fusion and binucleate heterokaryon formation in multiple sclerosis cerebellum. Brain : a journal of neurology. 2012 Oct;135(Pt 10):2962-72.

28. Al-Mahdawi S, Pinto RM, Varshney D, et al. GAA repeat expansion mutation mouse models of Friedreich ataxia exhibit oxidative stress leading to progressive neuronal and cardiac pathology. Genomics. 2006 Nov;88(5):580-90.

29. Anjomani Virmouni S, Sandi C, Al-Mahdawi S, Pook MA. Cellular, molecular and functional characterisation of YAC transgenic mouse models of Friedreich ataxia. PLoS One. 2014;9(9):e107416.

30. Greene E, Mahishi L, Entezam A, Kumari D, Usdin K. Repeat-induced epigenetic changes in intron 1 of the frataxin gene and its consequences in Friedreich ataxia. Nucleic Acids Res. 2007;35(10):3383-90.

31. Li K, Singh A, Crooks DR, et al. Expression of human frataxin is regulated by transcription factors SRF and TFAP2. PLoS One. 2010;5(8):e12286.

32. Shimizu R, Lan NN, Tai TT, et al. p53 directly regulates the transcription of the human frataxin gene and its lack of regulation in tumor cells decreases the utilization of mitochondrial iron. Gene. 2014 Nov 1;551(1):79-85.

33. Oktay Y, Dioum E, Matsuzaki S, et al. Hypoxia-inducible factor 2alpha regulates expression of the mitochondrial aconitase chaperone protein frataxin. J Biol Chem. 2007 Apr 20;282(16):11750-6.

34. Chantrel-Groussard K, Geromel V, Puccio H, et al. Disabled early recruitment of antioxidant defenses in Friedreich's ataxia. Human molecular genetics. 2001 Sep 15;10(19):2061-7.

35. Shan Y, Schoenfeld RA, Hayashi G, et al. Frataxin deficiency leads to defects in expression of antioxidants and Nrf2 expression in dorsal root ganglia of the Friedreich's ataxia YG8R mouse model. Antioxid Redox Signal. 2013 Nov 1;19(13):1481-93.

36. Sandi C, Sandi M, Jassal H, et al. Generation and Characterisation of Friedreich Ataxia YG8R Mouse Fibroblast and Neural Stem Cell Models. Plos One. 2014 Feb 21;9(2).

37. Peyronnard JM, Lapointe L, Bouchard JP, Lamontagne A, Lemieux B, Barbeau A. Nerve conduction studies and electromyography in Friedreich's ataxia. Can J Neurol Sci. 1976 Nov;3(4):313-7.

38. Santoro L, De Michele G, Perretti A, et al. Relation between trinucleotide GAA repeat length and sensory neuropathy in Friedreich's ataxia. Journal of neurology, neurosurgery, and psychiatry. 1999 Jan;66(1):93-6.

39. Jones J, Estirado A, Redondo C, et al. Mesenchymal stem cells improve motor functions and decrease neurodegeneration in ataxic mice. Mol Ther. 2015 Jan;23(1):130-8.

40. Pianese L, Turano M, Lo Casale MS, et al. Real time PCR quantification of frataxin mRNA in the peripheral blood leucocytes of Friedreich ataxia patients and carriers. J Neurol Neurosurg Psychiatry. 2004 Jul;75(7):1061-3.

41. Perdomini M, Belbellaa B, Monassier L, et al. Prevention and reversal of severe mitochondrial cardiomyopathy by gene therapy in a mouse model of Friedreich's ataxia. Nature medicine. 2014 May;20(5):542-7.

42. Libri V, Yandim C, Athanasopoulos S, et al. Epigenetic and neurological effects and safety of high-dose nicotinamide in patients with Friedreich's ataxia: an exploratory, open-label, dose-escalation study. Lancet. 2014 Aug 9;384(9942):504-13.

43. Yiu EM, Tai G, Peverill RE, et al. An open-label trial in Friedreich ataxia suggests clinical benefit with high-dose resveratrol, without effect on frataxin levels. J Neurol. 2015 May;262(5):1344-53.

44. Marcotulli C, Fortuni S, Arcuri G, et al. GIFT-1, a phase IIa clinical trial to test the safety and efficacy of IFNgamma administration in FRDA patients. Neurol Sci. 2016 Mar;37(3):361-4.

45. Mariotti C, Fancellu R, Caldarazzo S, et al. Erythropoietin in Friedreich ataxia: no effect on frataxin in a randomized controlled trial. Movement disorders : official journal of the Movement Disorder Society. 2012 Mar;27(3):446-9.

46. Paupe V, Dassa EP, Goncalves S, et al. Impaired nuclear Nrf2 translocation undermines the oxidative stress response in Friedreich ataxia. PLoS One. 2009;4(1):e4253.

47. D'Oria V, Petrini S, Travaglini L, et al. Frataxin deficiency leads to reduced expression and impaired translocation of NF-E2-related factor (Nrf2) in cultured motor neurons. Int J Mol Sci. 2013;14(4):7853-65.

48. Marmolino D, Manto M, Acquaviva F, et al. PGC-1alpha down-regulation affects the antioxidant response in Friedreich's ataxia. PLoS One. 2010;5(4):e10025.

49. Keller JN, Mattson MP. Roles of lipid peroxidation in modulation of cellular signaling pathways, cell dysfunction, and death in the nervous system. Reviews in the neurosciences. 1998;9(2):105-16.

50. Pollari E, Savchenko E, Jaronen M, et al. Granulocyte colony stimulating factor attenuates inflammation in a mouse model of amyotrophic lateral sclerosis. J Neuroinflammation. 2011;8:74.

51. Lledo PM, Alonso M, Grubb MS. Adult neurogenesis and functional plasticity in neuronal circuits. Nat Rev Neurosci. 2006 Mar;7(3):179-93.

52. Bolinches-Amoros A, Molla B, Pla-Martin D, Palau F, Gonzalez-Cabo P. Mitochondrial dysfunction induced by frataxin deficiency is associated with cellular senescence and abnormal calcium metabolism. Front Cell Neurosci. 2014;8:124.

53. Winner B, Kohl Z, Gage FH. Neurodegenerative disease and adult neurogenesis. The European journal of neuroscience. 2011 Mar;33(6):1139-51.

54. Toth ZE, Leker RR, Shahar T, et al. The combination of granulocyte colony-stimulating factor and stem cell factor significantly increases the number of bone marrow-derived endothelial cells in brains of mice following cerebral ischemia. Blood. 2008 Jun 15;111(12):5544-52.

55. Martinez C, Urbano-Ispizua A, Marin P, et al. Efficacy and toxicity of a high-dose G-CSF schedule for peripheral blood progenitor cell mobilization in healthy donors. Bone Marrow Transplant. 1999 Dec;24(12):1273-8.

Figure legends.

Fig 1. ***Neurological deficits in YG8R mice that carry a human genomic FXN transgene containing expanded GAA repeats of 82-190 units within intron 1 of the frataxin gene.*** **(A)** Experimental protocol using wild-type controls (WT) and YG8R mice to investigate the effects of cytokine administration on disease phenotype. Mice received monthly infusions of cytokines (red arrows) while also being assessed at monthly time points using an extensive range of behavioural performance tests. Bromodeoxyuridine (BrdU) was also administered during the last round of growth factor treatment (blue arrow). At 9 months of age neurophysiological evaluation of both sensory and motor nerve conduction was performed. Subsequently, mice were sacrificed for mRNA, protein and histological analysis. Comparisons between WT-control and untreated YG8R mice:- longitudinal results for **(B)** weight; **(C-G)** motor performance; and **(H)** locomotor performance (open field test), in mice from 3 to 9 months of age. Repeated measures (RM) two-way ANOVA was applied for all behavioural studies. ns (not significant), $*P < 0.05$,$**P < 0.01$, $***P < 0.001$, values represent means ± SEM. For all tests, $n = 10$ (5 female and 5 male) per genotype.

Fig 2. ***YG8R mice show gait abnormalities.*** Comparisons between WT-control and untreated YG8R mice:- (**A**) footprint (gait) analysis and (**B**) representative footprint traces in mice 9 months of age. The unpaired t-test was applied for all analysis. $*P < 0.05$,$**P < 0.01$, $***P < 0.001$, values represent means ± SEM. For all tests, $n = 10$ (5 female and 5 male) per genotype.

Fig 3. ***Treatment with G-CSF and/or SCF improves both motor and locomotor performance in YG8R mice.*** **(A)** The peripheral blood MNC counts of WT control and YG8R mice subcutaneously injected with G-CSF and/or SCF dissolved in PBS (200μg/kg body weight daily for 5 consecutive days). Longitudinal results for **(B)** weight; **(C-G)** motor performance; **(H)** locomotor performance (open field test); and **(I)** gait analysis, in YG8R mice treated with G-CSF and/or SCF, from 3 to 9 months of age. All statistical comparisons are vs YG8R mice using either the unpaired t-test, one-way or RM two-way ANOVA followed by Dunnett's multiple comparison test. ns (not significant), $*P < 0.05$, $**P < 0.01$, $***P < 0.001$, values represent means ± SEM. For all neurobehavioral tests, $n = 10$ (5 female and 5 male) per genotype.

Fig 4. ***Both frataxin and regulatory factors implicated in controlling frataxin transcription are elevated in the cerebellum and spinal cord of YG8R mice treated with G-CSF and/or SCF.*** **(A)** A schematic of the 5' end of the frataxin (*FXN*) gene showing the locations of the binding sites (yellow bars) for HIF-2A, SRF, TFAP2A and p53. The locations of the promotor (PR), Exon1, Exon2 and Intron1 regions are depicted. Different transcription start sites (TTS1 and TSS2) are shown upstream of Exon1, which holds the ATG translation start site. The directions of transcription for *FXN* (red arrows) and *FXN* anti-sense transcript (*FAST-1*; dashed black arrow) are shown. The red triangle indicates the site of the trinucleotide GAA repeat expansion within intron 1 of *FXN* gene of patients with FRDA. The relative **(B)** mRNA and protein expression levels of frataxin within the cerebellum and spinal cord of YG8R mice (normalised to NeuN or β actin); **(C)** mRNA expression levels of transcription factors implicated in controlling frataxin expression *Epas1*, *Srf*, *Tfap2a* and

Trp53 (normalised to NeuN). **(D)** The correlation and linear regression analysis of *FXN* and *Epas1* mRNA levels (normalised to NeuN) in the spinal cord and cerebellum of treated YG8R mice (lines of best fit and 95% CI are depicted), r = Spearman's correlation coefficient. All statistical comparisons are vs YG8R mice. Comparisons between control and untreated YG8R mice were analysed using unpaired t-tests or Mann-Whitney U tests. For all other analyses, either one-way ANOVA followed by Dunnett's multiple comparison test or Kruskal-Wallis followed by Dunn's multiple comparison test was applied for all analyses. $*P < 0.05$, $**P < 0.01$, $***P < 0.001$. For mRNA and protein expression, values represent the geometric means ± 95% CI and means ± SEM respectively. For all tests, $n = 4$ or 5 per genotype.

Fig 5. ***Neurophysiological deficits of the sensory nerve pathway are restored in YG8R mice treated with a combination of G-CSF and SCF.*** **(A)** Sensory compound nerve recording from the proximal tail after stimulation at the tail tip. **(B)** Motor compound nerve recording from the distal tail after stimulation of the proximal tail. The first small negative wave is due to antidromic activation of sensory fibres. **(A)** and **(B)** Responses are an average of 10 trials and from control animals. Arrowhead indicates the onset of the electrical stimulation. **(C)** Peak conduction velocities and durations of sensory and motor responses recorded from tails of wild type controls, untreated YG8R mice and YG8R mice treated with combined G-CSF/SCF. **(D)** The correlation and linear regression analysis of frataxin protein levels (normalised to NeuN) in the spinal cord and cerebellum of treated YG8R mice with either sensory nerve conduction velocity or wave duration (lines of best fit and 95% CI are depicted). All statistical comparisons are vs YG8R mice. One-way ANOVA followed by Dunnett's multiple comparison test was applied for all analyses. $*P < 0.05$, values represent

means ± SEM. Spearman's correlation was used to analyse relationships between frataxin and sensory nerve conduction velocity or wave duration. r = correlation coefficient.

Fig 6. ***G-CSF and SCF administration improves Friedreich's ataxia-associated pathology.*** **(A)** Haematoxylin and eosin-stained DRG depicting reductions in vacuolisation (red arrows) of large sensory neurons within YG8R mice treated with G-CSF/SCF. **(B)** High powered image of a DRG neuron showing significant vacuolisation (red arrow). **(C)** The frequency of DRG neurons containing vacuoles. **(D)** DRG sections labelled with NeuN and S100 showing auto-fluorescent lipofuscin (black arrow) and both intra-nuclear (white asterisk) and intra-cytoplasmic (white arrow) vacuolisation. **(E)** The DRG satellite-to-neuron cell ratio; **(F)** the size range and **(G)** mean cell size (diameter) of DRG neurons. **(H)** Images and **(I)** numbers of NeuN-labelled neurons within the DNoC of YG8R mice treated with G-CSF/SCF. **(J)** Images of Beta-3 tubulin-expressing neurons and **(K)** grumose-type GAD-positive intracytoplasmic labelling pattern in and around the large neuronal cell bodies within the dentate nucleus of control and YG8R mice. **(L)** The size range, **(M)** mean cell size (diameter) of Beta-3 tubulin-labelled neurons within the dentate nucleus. Comparisons between WT-control and YG8R mice were compared using the unpaired t-test. All other statistical comparisons are vs YG8R mice using either one-way ANOVA followed by Dunnett's multiple comparison test or Kruskal-Wallis followed by Dunn's multiple comparison test. $*P < 0.05$, $**P < 0.01$, $***P < 0.001$, values represent means ± SEM. For all tests, $n = 5$ per genotype.

Fig 7. ***G-CSF and SCF administration reduces glial/immune cell infiltration while stimulating the recruitment of neural precursors to areas of tissue injury.*** Numbers of **(A)** OX42- and **(C)** GFAP-positive cells within the spinal cord and dentate nucleus. **(B)**

Cerebellar sections depicting levels of OX42-positive cells in the dentate nucleus. **(D)** Spinal cord sections depicting levels of GFAP-positive cells within the spinal cord anterior corticospinal tract. Astrocytosis without loss of spinal cord white matter in YG8R mice observed using **(E)** luxol fast blue/cresyl violet staining and **(F)** MBP-dual immunolabelling with GFAP. **(G)** Spinal cord sections immunolabelled with GFAP and either MBP or 4-HNE, exhibiting astrocytosis, in both the white and grey matter, associated with 4-HNE accumulation. **(H)** Nestin cells/mm^2 and **(I)** images of nestin-positive cells within DRG, spinal cord and dentate nucleus. **(J)** BrdU cells/mm^2 within DRG, spinal cord and dentate nucleus. Dorsal column (DC), spinocerebellar tract (SCT), lateral corticospinal tract (LCST), anterior corticospinal tract (ACST), dentate nucleus of Clarke (DNoC). Comparisons between WT-control and YG8R mice were compared using the unpaired t-test. All other statistical comparisons are vs YG8R mice using either one-way ANOVA followed by Dunnett's multiple comparison test or Kruskal-Wallis followed by Dunn's multiple comparison test. *$P < 0.05$, **$P < 0.01$, ***$P < 0.001$, values represent means ± SEM. For all tests, $n = 5$ per genotype.

Tables.

Table 1. ***Friedreich's ataxia associated molecules and anti-oxidant defences are restored in both the cerebellum and spinal cord of YG8R mice treated with G-CSF and/or SCF.*** The relative protein expression levels of frataxin; aconitase enzyme activity; transcription factors Nrf2 and PGC1A; anti-oxidant enzymes SOD1, SOD2, catalase and GPX1, and lipid peroxidation product 4-HNE, within the cerebellum and spinal cord of both WT controls and YG8R mice and YG8R mice treated with G-CSF and/or SCF. All statistical comparisons are

vs YG8R mice. Comparisons between control and untreated YG8R mice were analysed using unpaired t-tests or Mann-Whitney U tests. For all other analyses, either one-way ANOVA followed by Dunnett's multiple comparison test or Kruskal-Wallis followed by Dunn's multiple comparison test was applied for all analyses. *$P < 0.05$, **$P < 0.01$, ***$P < 0.001$. Values represent the mean ± SEM, relative to values in untreated YG8R mice. For all tests, $n = 5$ per genotype.

Protein	Site	Level relative to	Control	YG8R	YG8R + G-CSF	YG8R + SCF	YG8R + SCF/G-CSF
Friedreich's ataxia associated molecules							
Nrf2	cerebellum	total protein	**1.40 (0.08)****	1.00 (0.05)	1.12 (0.09)	**1.40 (0.18)***	**1.45 (0.10)***
		NeuN	**1.27 (0.02)***	1.00 (0.09)	**1.66 (0.17)****	**1.54 (0.13)***	**1.50 (0.11)***
	spinal cord	total protein	0.95 (0.05)	1.00 (0.07)	0.85 (0.10)	1.19 (0.11)	1.08 (0.11)
		NeuN	1.61 (0.26)	1.00 (0.16)	**2.06 (0.26)***	1.88 (0.33)	**2.06 (0.16)***
PGC-1a	cerebellum	total protein	**1.45 (0.08)*****	1.00 (0.04)	1.23 (0.10)	1.31 (0.10)	**1.38 (0.09)***
		NeuN	**1.30 (0.02)***	1.00 (0.08)	**1.81 (0.18)****	1.45 (0.13)	1.43 (0.14)
	spinal cord	total protein	**1.18 (0.04)***	1.00 (0.06)	1.06 (0.07)	**1.38 (0.09)****	1.20 (0.08)
		NeuN	**1.96 (0.40)***	1.00 (0.20)	**2.46 (0.25)****	**2.09 (0.30)***	**2.26 (0.26)****
Aconitase	cerebellum	total protein	**1.76 (0.12)*****	1.00 (0.06)	1.22 (0.16)	1.11 (0.10)	**1.61 (0.10)****
		NeuN	**1.54 (0.16)****	1.00 (0.07)	**1.72 (0.02)****	1.24 (0.11)	**1.70 (0.12)****
	spinal cord	total protein	1.03 (0.11)	1.00 (0.10)	1.79 (0.38)	0.94 (0.20)	1.83 (0.14)
		NeuN	1.70 (0.35)	1.00 (0.27)	**4.07 (0.87)****	1.29 (0.23)	**3.36 (0.34)***
Anti-oxidant enzyme/oxidative damage expression							
SOD1	cerebellum	total protein	**1.37 (0.05)****	1.00 (0.05)	1.17 (0.08)	**1.28 (0.07)***	1.22 (0.08)
		NeuN	**1.22 (0.03)***	1.00 (0.06)	**1.74 (0.15)****	1.44 (0.15)	1.27 (0.10)
	spinal cord	total protein	**1.42 (0.11)***	1.00 (0.06)	1.01 (0.11)	**1.54 (0.06)****	1.40 (0.18)
		NeuN	**2.28 (0.31)****	1.00 (0.20)	**2.30 (0.18)****	**2.32 (0.31)****	**2.60 (0.34)****
SOD2	cerebellum	total protein	1.30 (0.12)	1.00 (0.08)	1.34 (0.07)	**1.72 (0.13)*****	1.32 (0.14)
		NeuN	1.19 (0.11)	1.00 (0.07)	**2.01 (0.22)****	**1.97 (0.28)****	1.37 (0.13)
	spinal cord	total protein	1.39 (0.24)	1.00 (0.05)	**2.21 (0.14)*****	**2.76 (0.26)*****	**1.79 (0.20)***
		NeuN	2.07 (0.25)	1.00 (0.23)	**4.94 (0.43)****	**3.96 (0.46)***	**3.67 (1.16)***
Catalase	cerebellum	total protein	**1.57 (0.13)****	1.00 (0.05)	1.23 (0.06)	**1.42 (0.06)****	**1.31 (0.12)***
		NeuN	**1.45 (0.08)****	1.00 (0.05)	**1.84 (0.19)****	**1.63 (0.21)***	1.35 (0.10)
	spinal cord	total protein	**1.40 (0.19)***	1.00 (0.06)	**1.75 (0.12)*****	**2.04 (0.13)*****	**1.62 (0.12)****

		NeuN	**1.84 (0.06)***	1.00 (0.23)	**3.96 (0.47)*****	**2.95 (0.37)***	**3.09 (0.64)***
GPX1	cerebellum	total protein	**1.30 (0.08)***	1.00 (0.07)	1.21 (0.11)	**1.40 (0.05)***	**1.39 (0.12)***
		NeuN	1.51 (0.32)	1.00 (0.06)	**1.78 (0.10)*****	**1.59 (0.12)*****	**1.44 (0.08)***
	spinal cord	total protein	0.93 (0.05)	1.00 (0.10)	0.91 (0.03)	1.25 (0.04)	1.30 (0.15)
		NeuN	1.69 (0.29)	1.00 (0.13)	**2.29 (0.25)****	**2.02 (0.23)***	**2.06 (0.26)***
4-HNE	cerebellum	total protein	**0.55 (0.02)***	1.00 (0.13)	0.74 (0.06)	0.95 (0.02)	**0.67 (0.09)***
		NeuN	n/a	n/a	n/a	n/a	n/a
	spinal cord	total protein	**0.54 (0.08)***	1.00 (0.11)	0.88 (0.10)	0.85 (0.12)	0.67 (0.06)
		NeuN	n/a	n/a	n/a	n/a	n/a

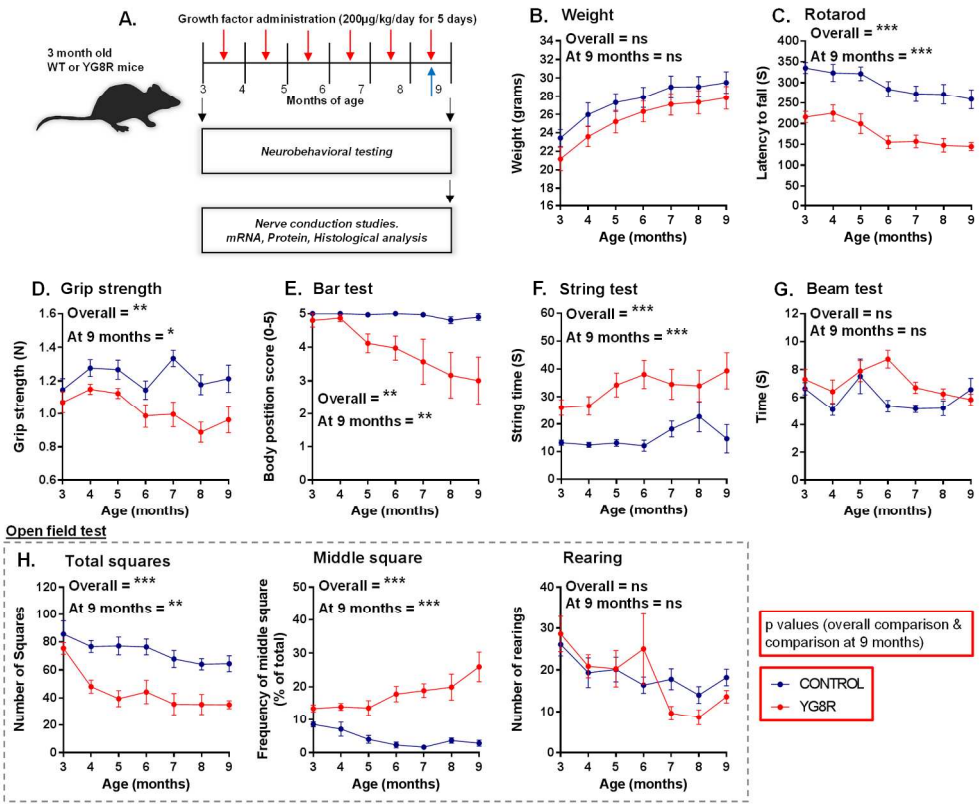

Fig 1
170x140mm (300 x 300 DPI)

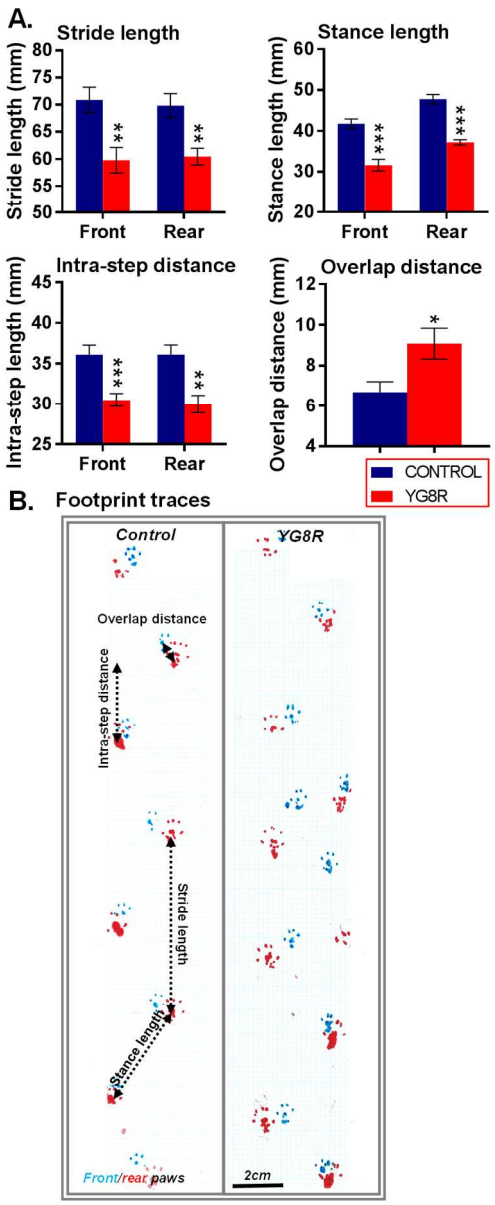

Fig 2
80x188mm (300 x 300 DPI)

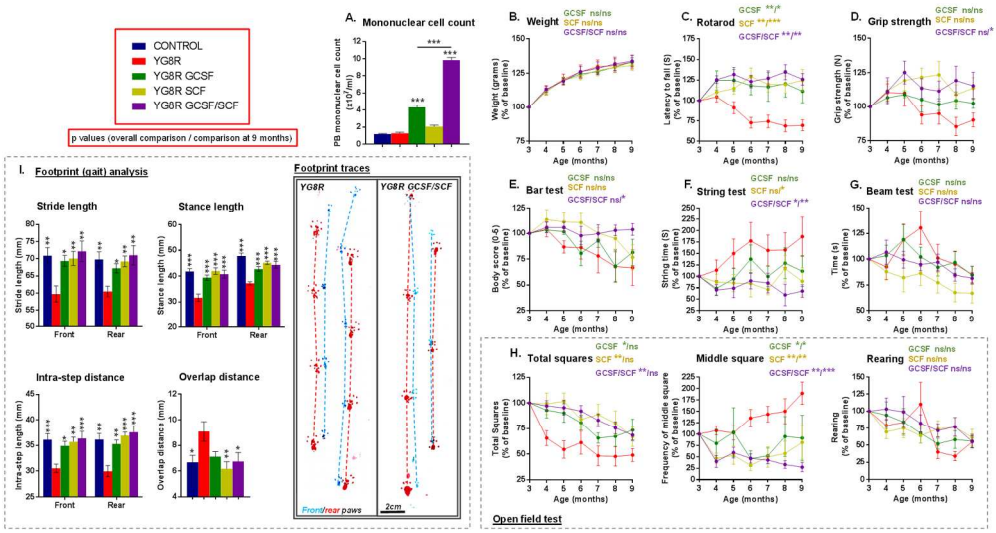

Fig 3
170x91mm (300 x 300 DPI)

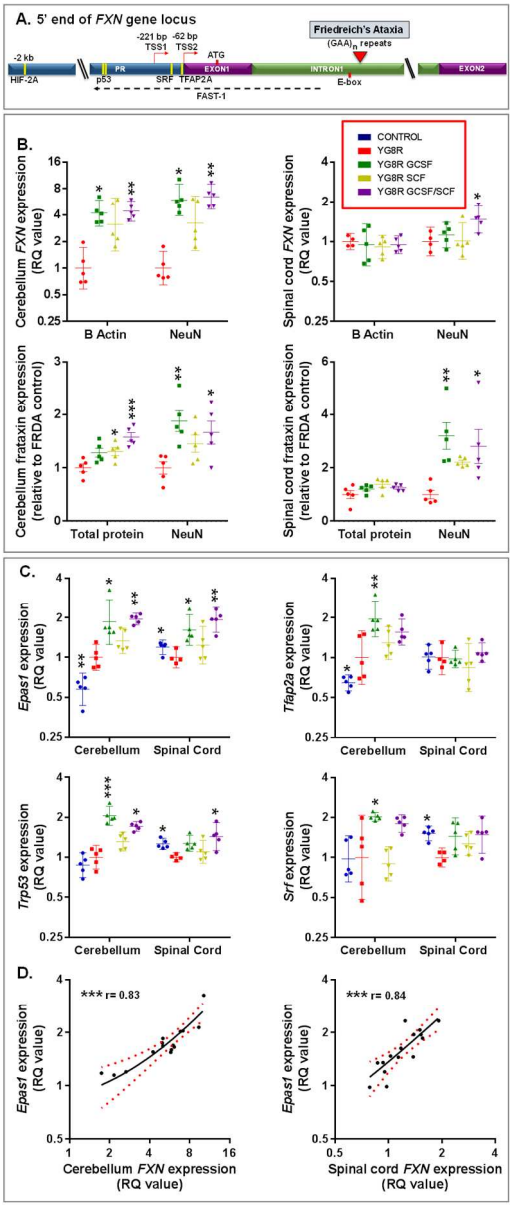

Fig 4
80x189mm (300 x 300 DPI)

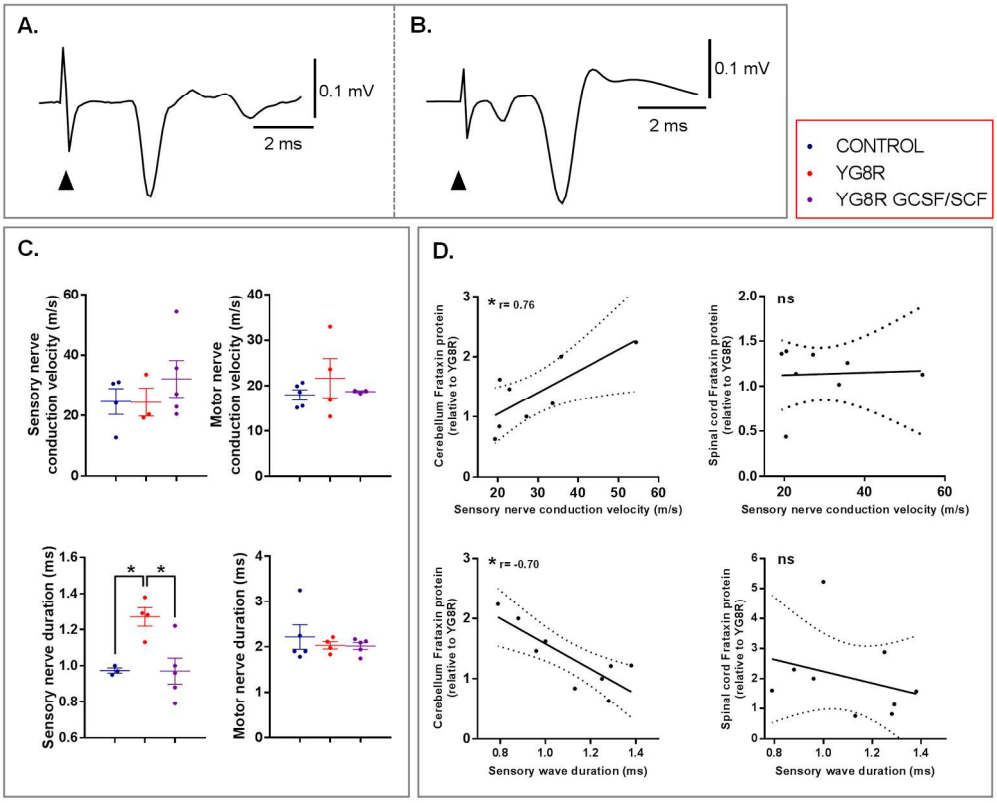

Fig 5
170x137mm (300 x 300 DPI)

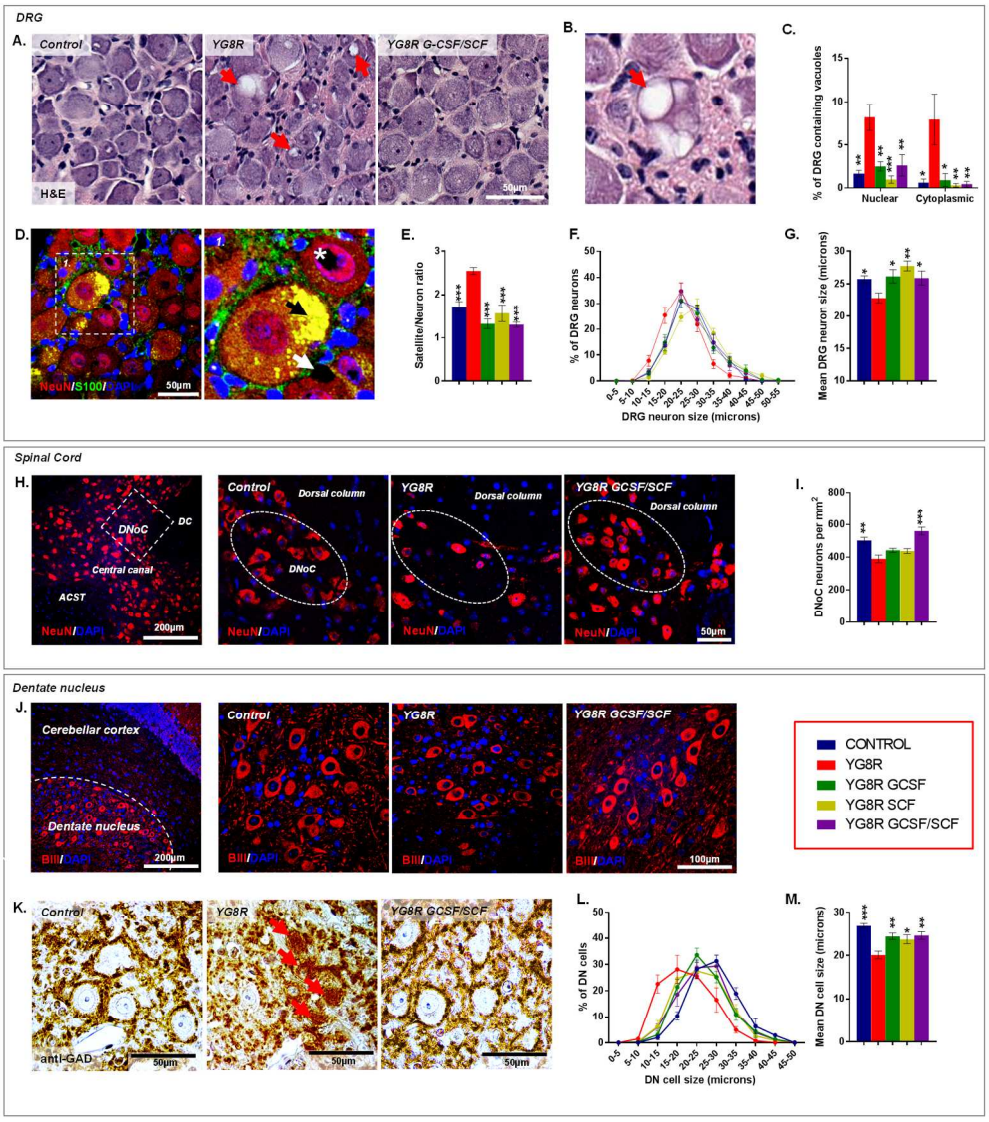

Fig 6
170x189mm (300 x 300 DPI)

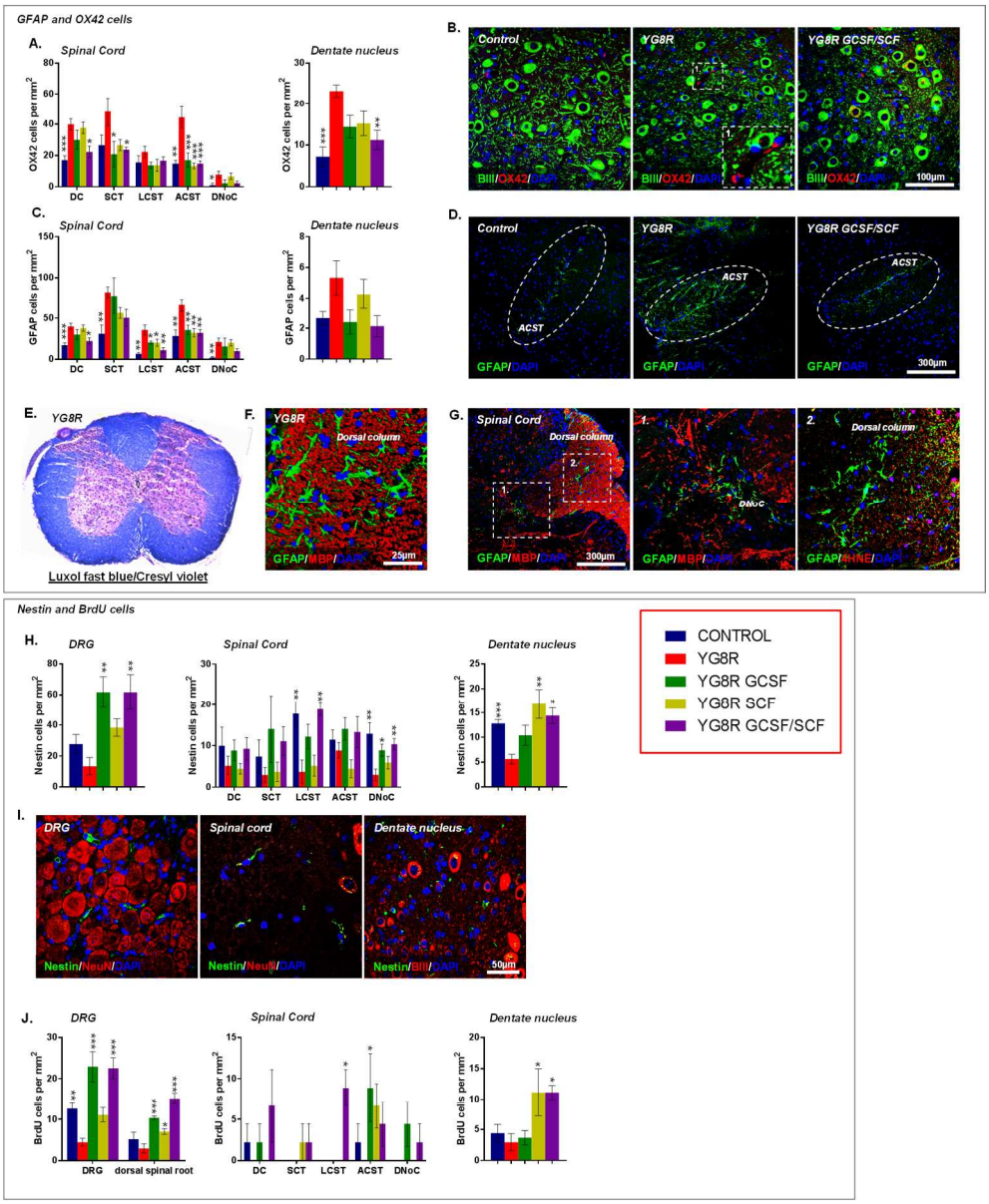

Fig 7
170x207mm (300 x 300 DPI)